IRAP+ endosomes restrict TLR9 activation and signaling

Joël Babdor, Delphyne Descamps, Aimé Cézaire Adiko, Mira Tohmé, Sophia Maschalidi, Irini Evnouchidou, Luiz Ricardo Vasconcellos, Mariacristina de Luca, Francois-Xavier Mauvais, Meriem Garfa-Traore, et al.

IRAP endosomes restrict TLR9 activation and signaling

Joel Babdor[1,2,3&], Delphyne Descamps[1,2,3,4&], Adiko Assi Aimé Cézaire[9,10], Mira Tohmé[1,2,3,5], Sophia Maschalidi[1,2,3], Irini Evnouchidou[9,10], Luiz Vasconcellos[1,2,3], Mariacristina De Luca[9,10], Francois-Xavier Mauvais[1,2,3], Meriem Garfa-Traore[1,2,3], Melanie M. Brinkmann[8], Michel Chignard[6,7], Bénédicte Manoury[1,2,3*], Loredana Saveanu[9,10*]

1. Institut National de la Santé et de la Recherché Médicale, Unité 1151, Paris, 75015, France
2. Centre National de la Recherche Scientifique, Unité 8253, Paris, 75015, France
3. Université Paris Descartes, Sorbonne Paris Cité, Faculté de médecine Paris Descartes, 75015 Paris, France
4. VIM, INRA, Université Paris-Saclay, 78350, Jouy-en-Josas, France.
5. Institut National de la Santé et de la Recherché Médicale, Unité 932, Institut Curie, 75005, Paris, France
6. Institut National de la Santé et de la Recherché Médicale, UMR S 938, CDR Saint-Antoine, Paris, France
7. Sorbonne Université, UPMC Univ Paris 06, UMR S 938, CDR Saint-Antoine, Paris, France
8. Helmholtz Centre for Infection Research, 38124 Braunschweig, Germany
9. Institut National de la Santé et de la Recherché Médicale, Unité UMR 1149, Centre de Recherche sur l'Inflammation, Paris, France
10. Université Paris Diderot, Faculté de Médecine Xavier Bichat, Paris, France

[&] These authors contributed equally to this work

* Co-senior authors

[*] **Corresponding authors**:
Loredana Saveanu, INSERM, Unité 1149, Faculté de Médecine Bichat, 16 rue Henri Huchard, 75018, Paris cedex 18, France
Bénédicte Manoury, INSERM, Unité 1151, Hôpital Necker-Enfants malades, 149 rue de Sèvres, 75743 Paris cedex 15, France
Emails: loredana.saveanu@inserm.fr, benedicte.manoury@inserm.fr

Abstract

Retention of intracellular Toll-Like Receptors (TLRs) in the endoplasmic reticulum prevents their activation under basal conditions. TLR9, whose trafficking is still largely unknown, is activated by sensing ligands in specific endosomal compartments. Here, we describe the identification of IRAP (insulin responsive aminopeptidase) vesicles as major cellular compartments for the early steps of TLR9 activation in dendritic cells (DCs). Both CpG and TLR9 were found to be cargos of IRAP endosomes. In the absence of IRAP, CpG and TLR9 trafficking to lysosomes and TLR9 signaling were enhanced in DCs and in mice following bacterial infection. IRAP stabilized CpG-containing endosomes by interacting with the actin nucleation factor FHOD4, slowing down TLR9 activation in lysosomes. Thus, endosome retention through IRAP interaction with the actin cytoskeleton is a mechanism that prevents TLR9 hyper-activation in DCs.

Innate and adaptive immune responses depend on the ability of toll-like receptors (TLRs) to discriminate between different classes of microbial products and initiate specific signaling cascades. While microbial products with no equivalent in mammalian cells, such as the components of the bacterial wall, are recognized by surface TLRs (1, 2, 4, 5 and 6), pathogen derived nucleic acids are sensed by intracellular TLRs (3, 7, 8 and 9). Recognition of nucleic acids by intracellular TLRs has an intrinsic potential to trigger autoimmune diseases through interaction with self nucleic acids [1]. To avoid inappropriate activation of endosomal TLRs, the trafficking of these receptors is tightly controlled. Thus, in basal conditions the receptors are located in the endoplasmic reticulum (ER) and translocate to endocytic vesicles only after cell stimulation by TLR ligands. Although all intracellular TLRs reside in the ER and require the chaperone Unc93b for their transfer to endosomes [2,3], the trafficking pathways that move the receptors into the endocytic pathway show considerable variation among intracellular TLRs [4-6]. For example, the TLR7/Unc93b complex traffics from Golgi stacks directly to endosomes using the clathrin adaptor AP4, while the TLR9/Unc93b complex is directed to the cell surface and reaches the endosomes via AP2-mediated clathrin-dependent endocytosis [6].

In addition to the transfer into the endocytic pathway, a second step that controls the activation of endosomal TLRs is their partial proteolysis by an array of different proteases, specific for each TLR [5,7-12].

Although less often mentioned, the intracellular trafficking of its ligand also controls the activation of TLR9. TLR9 ligands (CpG) are internalized via clathrin-mediated endocytosis in early endosomes and translocate to late $LAMP^+$ compartments [2]. TLR9 activation depends on CpG localization, since the abrogation of CpG translocation to $LAMP^+$ vesicles by PIKfyve inhibitors decreased TLR9 signaling [13,14]. Thus, the intracellular trafficking of both, the ligand and the receptor are essential for the control of TLR9 activation.

The complexity of TLR9 and CpG trafficking is rendered possible by the diversity and plasticity of the endocytic system. This system includes early endosomes that fuse to generate the sorting endosomes. From there, cargos are directed to different organelles, such as $Rab4^+$ fast recycling endosomes, $Rab11^+$ slow recycling endosomes, the trans Golgi network (TGN) or lysosomes. Next to these universal routes of endosome trafficking, specialized cells, such as dendritic cells (DCs), display particular, albeit poorly characterized endosomal populations that affect TLR function, such as the $VAMP3^+$ vesicles, which are involved in TLR9 trafficking [15].

A particular and abundant endocytic population present in DCs, not yet investigated in the context of TLR signaling, is the slow recycling endosomes. They are characterized by the presence of the aminopeptidase IRAP (Insulin Responsive AminoPeptidase), a type II transmembrane protein composed of a catalytic site localized in the endosomal lumen and a cytosolic domain of 110 amino acids. We have previously demonstrated that in DCs, IRAP$^+$ vesicles are rapidly recruited to DC phagosomes, where the enzymatic activity of IRAP is involved in antigen processing during MHC-I cross presentation [16,17].

In addition to DCs, IRAP$^+$ endosomes have been extensively studied in adipocytes, were they are called Glut4 storage vesicles (GSVs) and are rapidly transported to the cell surface under insulin stimulation. After the fusion of the endosomes with the cell membrane, Glut4 remains at the cell surface to facilitate glucose uptake, while IRAP is rapidly internalized [18]. Thus, both in adipocytes and in DCs, IRAP displays a complex trafficking, sensitive to external regulation by insulin or phagocytic receptors activation. The regulated trafficking of IRAP depends on the cytosolic domain of the enzyme, which has been shown to interact with several proteins involved in vesicles formation or in cytoskeleton remodeling, such as the golgin p115 [19], vimentin [20] and FHOS (formin homologue overexpressed in the spleen, also called FHOD1) [21]. Whether these proteins and their interaction with the cytosolic domain of IRAP play a role in the complex trafficking of IRAP and IRAP$^+$ endosomes is not known.

Considering the dynamic and potentially regulated nature of IRAP$^+$ endosomes, we wondered if IRAP plays a role in endosomal TLR trafficking and activation. We report here that the early step in TLR9 trafficking and CpG endocytosis requires IRAP. The absence of IRAP affects both CpG and TLR9 trafficking, leading to a dramatic increase in TLR9 signaling *in vitro* and *in vivo* following TLR9 stimulation. These results can be explained by the central role of IRAP in anchoring TLR9 endosomes to the actin cytoskeleton, which would limit TLR9-driven inflammatory responses. These findings provide a mechanistic explanation to the link between IRAP mutations and autoimmune disorders implicating TLR9 [22] and identify new factors and cellular pathways involved in TLR9 activation.

RESULTS

IRAP deletion increases TLR9 response

To address the role of IRAP in TLRs signaling, wild type (wt) and IRAP-deficient (ko) bone marrow derived dendritic cells (BM-DCs) were stimulated with ligands specific for intracellular and membrane TLRs: polyIC for TLR3, Imiquimod for TLR7, CpG-B for TLR9

and LPS for TLR4, and the production of the pro-inflammatory cytokines IL-6, IL-12p40, TNF □□□□□□□□□□□□□. While IRAP deletion did not affect TLR3- and TLR4-dependent pro-inflammatory cytokine production, it enhanced pro-inflammatory cytokine production driven by TLR9 (**Fig. 1a**) and TLR7 activation (**Supplementary Fig. 1a**). These results suggest that IRAP affects the NF-κB pathway downstream of TLR9 and probably TLR7.

Since type I IFN production depends on TLR9 signaling through IRF-7, we wondered whether IRAP deletion affected this cytokine. We measured IFN-β production by wt and IRAP-deficient BM-DCs stimulated with TLR3, 4 and 9 ligands (**Fig. 1b**). IRAP deletion significantly increased only TLR9-driven IFN-β production but not IFN-β production by TLR3 and TLR4. Thus, IRAP disturbed the amplitude of both pro-inflammatory cytokine and type I IFN production in a TLR9-dependent manner in BM-DCs.

To address whether the hypersensitivity of IRAP-deficient cells to TLR9 ligands was restricted to BM-DCs, which correspond to monocyte-derived inflammatory DCs, we purified conventional DCs (cDCs) and plasmacytoïd DCs (pDCs) from the spleen and stimulated them with a TLR9 agonist. When incubated with CpG, IRAP-deficient spleen cDCs (**Fig. 1c**) and pDCs (**Fig. 1d**) produced significantly higher amounts of pro-inflammatory cytokines and INF-α than their wt counterparts. These results demonstrated that IRAP expression was required to prevent exacerbated inflammatory cytokine production in response to TLR9 activation in all tested DC subsets.

At least two mechanisms might account for the increased TLR9 response in IRAP-deficient DCs. $IRAP^+$ vesicles, which are storage compartments sensitive to regulation by cell-specific stimulation in adipocytes, could store pro-inflammatory cytokines and control their trafficking and secretion. Alternatively, $IRAP^+$ endosomes could directly influence TLR9 or CpG trafficking. We thus analyzed the intracellular localization of pro-inflammatory cytokines in wt and IRAP-deficient cells. While both IL-6 and IL-12 could not be detected in unstimulated cells, incubation with CpG resulted in staining for IL-6 and IL-12 in intracellular structures with a morphology indicative of Golgi stacks but devoid of IRAP staining (**Supplementary Fig. 1b**). The staining for the cis-Golgi matrix protein GM130, consistent with previous reports, confirmed IL-6 localization in Golgi stacks (**Supplementary Fig. 1c**)[23].

Thus, $IRAP^+$ endosomes are unlikely to be implicated in trafficking or secretion of IL-6 or IL-12(p40) and could be involved in a step upstream their synthesis. In support to this hypothesis, we found that DCs lacking IRAP expressed significantly higher levels of pro-inflammatory cytokine mRNAs than wt DCs upon CpG but not LPS stimulation (**Fig. 1e-f**).

The increase in cytokines, both at the mRNA and protein level, in IRAP deficient cells following TLR9 stimulation should be correlated with an enhanced TLR9 signaling. To specifically investigate TLR9 signaling, we tested the association of the MyD88 adaptor with the transcription factors NF-κB and IRF7. The proximity ligation assay (Duolink), which detects protein complexes *in situ* [24], demonstrated a significantly increased association of MyD88 with NF-κB (**Fig. 2a**) and of MyD88 with IRF7 (**Fig. 2b**) in IRAP-deficient cells, as compared with wt cells.

As a consequence of TLRs activation, the mitogen-activated protein kinase ERK is rapidly phosphorylated. Indeed, ERK phosphorylation was increased in IRAP deficient cells after CpG stimulation, as detected by immunoblot (**Fig. 2c**). In addition, the last step of NF-κB activation, the phosphorylation of IκB-α, was also significantly increased in IRAP-deficient cells after CpG but not LPS treatment (**Fig. 2d**), indicating an enhanced TLR9 signaling in the absence of IRAP.

IRAP-deficient mice display a hyper-inflammatory phenotype driven by TLR9 activation

Our *in vitro* data demonstrated the regulation of TLR9 signaling by IRAP. We next addressed the question whether IRAP-deficient mice display increased TLR9 activation. To test this, we measured the level of IL-6 in the serum of wt and IRAP-deficient mice 2 h after intravenous injection of PBS, CpG-B or LPS. While wt and IRAP-deficient animals responded identically to PBS and LPS injection, TLR9 stimulation led to higher levels of IL-6 in the serum of mice lacking IRAP than in wt animals (**Fig. 3a**).

We wondered if the observed exacerbated pro-inflammatory TLR9 signaling might affect the innate immune response during a bacterial infection. *Pseudomonas aeruginosa (P. aeruginosa)* is an opportunistic Gram-negative bacterium that activates several TLRs including TLR9 on alveolar macrophages (AM) and epithelial cells [25]. TLR9-deficient mice were recently shown to be resistant to *P. aeruginosa* infection, suggesting that TLR9 signaling can have deleterious effects in this model [26]. In order to test whether the TLR9-dependent hyper-activation observed in IRAP-deficient mice could affect survival upon bacterial pulmonary infection, we intranasally inoculated IRAP-deficient and wt mice with 10^6 cfu of *P. aeruginosa* and monitored them for survival. At least 36% of wt mice survived during the two weeks of observation, while all IRAP-deficient mice died within 72 h after infection (**Fig. 3b**). We then investigated the correlation between mice survival and the

inflammatory response monitored in the lungs 24 h post-infection. In infected IRAP-deficient mice, broncho-alveolar lavage (BAL) fluid contained higher levels of KC, IL-6, TNF-α and IL-1β than in wt mice (**Fig. 3c**). Since AMs are the first innate immune cells to encounter bacteria in the lungs, we isolated AM and tested their cytokine production upon TLR9 and TLR4 stimulation *in vitro*. While a response was barely detectable in AM isolated from wt mice, IRAP-deficient AMs secreted substantial higher amounts of all pro-inflammatory cytokines tested upon CpG stimulation (**Fig. 3d**) in comparison to wt mice. In contrast, IRAP deficiency did not alter IL-6 and TNF-α secretion upon LPS stimulation, indicating that the hyper-inflammatory phenotype produced was restricted to TLR9 (**Fig. 3d**).

To control for a potential difference between the two mouse strains in their ability to clear bacteria from the lungs, we measured the pulmonary bacterial load and found it to be identical in IRAP-deficient and wt mice (**Fig. 3e**). Consistent with an identical ability of both strains to clear bacteria, *P. aeruginosa* infection led to a similar accumulation of neutrophils and macrophages/monocytes in the airways of both groups (**Supplementary Fig. 2a**). In addition, myeloperoxidase activity that mirrors neutrophil degranulation was similar in BALs from both wt and IRAP-deficient mice (**Supplementary Fig. 2b**). Altogether, these experiments suggest that following *P. aeruginosa* infection, IRAP-deficient mice died earlier probably because of an excessive inflammatory response driven by TLR9 hyper-stimulation.

IRAP enzymatic activity is not involved in TLR9 activation

Our results showed that proper regulation of TLR9 signaling required IRAP. Since IRAP is an aminopeptidase, we wondered if the enzymatic activity of IRAP was involved in the control of TLR9 activation. To investigate this possibility, we tested the effect of an inactive form of IRAP on TLR9 activation. IRAP, similar to all M1 aminopeptidases, has a Zn^{2+} atom in the active site [27] and contains the canonical zinc-binding amino acid motif HELAH, which is essential for the enzymatic activity. A form of IRAP in which the HELAH sequence was changed into HALAH (E465A substitution) co-localized, like the wild-type protein, with syntaxin 6 (Stx6), a SNARE of $IRAP^{+}$ vesicles [16,17] (**Fig. 4a**). Both the wt and mutated form of IRAP were well expressed, as shown by immunoblotting with anti-IRAP antibodies (**Fig. 4b**) but the mutated form was enzymatically inactive (**Fig. 4c**). When we reconstituted IRAP-deficient BM-DCs with wild-type IRAP (**Fig. 4d**) or enzymatically inactive IRAP (**Fig. 4e**), pro-inflammatory cytokine production upon CpG stimulation was similar to wt cells. These results demonstrated that the enzymatic activity of IRAP is not involved in the control of TLR9 activation.

CpG and TLR9 are cargos of IRAP vesicles

Since IRAP enzymatic activity was not involved in TLR9 activation, we wondered if IRAP could interfere directly with TLR9 or CpG trafficking. Analysis of CpG-FITC by confocal microscopy demonstrated that CpG massively colocalized with IRAP. After 20 min of endocytosis, half of the internalized CpG was found in IRAP vesicles, where it was retained for at least 1 h (**Fig. 5a**). Concomitant with IRAP-CpG colocalization, we observed a significant increase of co-localization between IRAP and TLR9-GFP (**Fig. 5b**). While only 20% of TLR9 was found in IRAP vesicles early after CpG stimulation, the TLR9 ligand was a major and persistent cargo of IRAP endosomes.

Since both TLR9 and its ligand trafficked via IRAP vesicles, we wondered if IRAP vesicles overlap with VAMP3, a marker of an endosomal population through which TLR9 traffics towards lysosomes [15]. IRAP, as well as the small GTPase Rab14 and the Q-SNARE Stx6, two others markers of $IRAP^+$ vesicles in DCs [16,17] coincided with VAMP3 endosomes (**Supplementary Fig. 3**). These results suggest that IRAP vesicles are a new intermediate compartment between early endosomes and the final destination of TLR9, which is the $LAMP^+$ lysosome. This conclusion is also supported by the absence of colocalization between IRAP and LAMP that we have shown previously [16,17].

IRAP absence increases the susceptibility of TLR9 to lysosomal processing

Since CpG and TLR9 are cargos of IRAP vesicles, we wondered if IRAP deletion could change the trafficking of CpG and TLR9. Analysis of CpG-FITC trafficking demonstrated that the proportion of TLR9 ligand transported to $LAMP^+$ vesicles was significantly higher in IRAP-deficient cells than in wt cells, an effect that was obvious at early time points (**Fig. 6a**). The accelerated transport to lysosomes of CpG, in IRAP-deficient DCs, was potentially correlated with a change in the intracellular distribution of TLR9-GFP, which was found in lysosomes even in the absence of CpG stimulation (**Fig. 6b**). The presence of TLR9 in the $LAMP^+$ compartment correlates with proteolytic generation of a highly active C-terminal fragment of the receptor in DCs and macrophages [7,8,11,12,28]. In agreement with the lysosomal localization of TLR9 in unstimulated IRAP-deficient cells, we found that in IRAP-deficient, but not in wt primary mouse embryonic fibroblasts transfected with TLR9-GFP and UNC93B-Cherry, the majority of immunoprecipitated TLR9-GFP corresponded to its processed form (**Fig. 6c**). As expected from the functional assays of TLR stimulation (**Fig. 1a-b**), TLR3 did not colocalize with IRAP and intracellular localization of TLR3 was not

affected by IRAP deletion (**Supplementary Fig. 4**). Thus, in the absence of IRAP, TLR9, but not TLR3, was targeted to lysosomes without cell stimulation.

To ensure that the lysosomal expression of TLR9 in IRAP-deficient cells was not the consequence of TLR9-GFP expression by nucleofection, we investigated the localization of endogenous TLR9. Since the only antibody that is specific for TLR9 (**Fig. 6d**) was not sensitive enough to detect TLR9 in whole cell lysate, we isolated early and late phagosomes from wt and IRAP-deficient DCs. While in the absence of CpG, TLR9 was not recruited to phagosomes in wt cells, we detected the active C-terminal form of TLR9 in IRAP-deficient late phagosomes. Thus, similar to the TLR9-GFP fusion, endogenous TLR9 was recruited to phago-lysosomes without CpG treatment in the absence of IRAP. Intriguingly, when the cells were stimulated with CpG, TLR9 recruitment to early and late phagosomes was identical between wt and IRAP-deficient cells (**Fig. 6e**). However, despite the similar recruitment to phago-lysosomes of endogenous TLR9 in both wt and IRAP-deficient cells upon CpG treatment, TLR9 signaling was exacerbated only in IRAP-deficient cells. This apparent contradiction can be explained by an increased accessibility of TLR9 to CpG in IRAP-deficient cells, suggested by the accelerated translocation of internalized CpG-FITC to lysosomes (**Fig. 6a**).

IRAP deletion reduces CpG and TLR9 retention in early endosomes

Since the consequences of IRAP on TLR9 hyper-activation could come from properties of IRAP on early endosome trafficking, we wondered if the early steps of CpG and TLR9 trafficking were modified by IRAP depletion. To analyze this, we used the early endosomal antigen, EEA1, a tethering factor known to be involved in homotypic and heterotypic fusion events of early endosomes. EEA1 recruitment to endosome is a mandatory step in endosome maturation to lysosome since inhibition of EEA1 activity blocks phagosome maturation [29]. Nevertheless, a fraction of $EEA1^+$ vesicles display a slow maturation rate and do not fuse rapidly to late endosomes [30]. To visualize TLR9 and CpG trafficking in $EEA1^+$ vesicles, we used BM-DCs from TLR9-GFP transgenic mice pulsed with CpG-biotin (**Fig. 7a**) in which IRAP was depleted by lentiviral shRNA (shIRAP) delivery (**Fig. 7d**). Colocalization analysis between TLR9-GFP and EEA1 showed that in IRAP-depleted cells, and not in control cells (shNT), TLR9 displayed a vesicular staining in subdomains of EEA1 endosomes in the absence of CpG (**Fig. 7a**, upper panels). Following CpG incubation, the trafficking of CpG was also affected by IRAP depletion. While in control cells, 25% of internalized CpG remained in EEA1 endosomes for 2 h, in IRAP-depleted cells, CpG was rapidly transferred

294 from EEA1^{+} vesicles to TLR9^{+} vesicles, as illustrated by the white arrow in the **Fig. 7a**,
295 middle panel. As a consequence of the rapid transfer to TLR9^{+} vesicles in IRAP-depleted
296 cells, the colocalization between CpG and TLR9 was 3 times higher in comparison to control
297 cells (**Fig. 7b**). This enhanced localization of CpG in TLR9 positive vesicles in cells lacking
298 IRAP was not the consequence of an increased up-take of CpG by IRAP-depleted cells (**Fig.**
299 **7c**).
300 Thus, IRAP depletion facilitated not only TLR9 processing but also TLR9 access to its
301 ligand.
302
303 **IRAP interaction with the FHOD4 formin provides a molecular mechanism for the**
304 **control of TLR9 activation**
305 Altogether, these results highlighted a role for IRAP in TLR9 and CpG retention in EEA1^{+}
306 endosomes that was independent on its enzymatic activity. We reasoned that the effect of
307 IRAP on TLR9 activation could be mediated by interactions with proteins that play roles in
308 vesicular trafficking. Two cytoskeleton factors have been previously identified to interact
309 with the cytosolic domain of IRAP: vimentin [20] and FHOD1 (formin homology domain-
310 containing proteins; synonym: FHOS-formin homologue overexpressed in the spleen) [21].
311 Vimentin forms intermediate filaments, cytoskeleton components that are important for
312 anchoring intracellular organelles [31]. FHOD formins are proteins essential for actin
313 polymerization and are involved in anchoring vesicles to the actin cytoskeleton [32]. Thus,
314 vimentin and formins could play a role in the control of IRAP-mediated trafficking of TLR9.
315 Duolink and co-immunoprecipitation experiments in fibroblasts and in DCs failed to show a
316 robust interaction between IRAP and vimentin (data not shown), which implies that the
317 IRAP-vimentin interaction that has been demonstrated in adipocytes [20] might be specific to
318 that cell type.
319 To investigate the FHOD1-IRAP interaction in DCs, we first investigated the expression of
320 FHOD1 in different cell types as reported in the gene expression database of the ImmGen [33]
321 consortium (**Fig. 8a**). The mRNA expression data recovered from ImmGen
322 (https://www.immgen.org/Databrowserpage.swf) showed that while FHOD1 expression is
323 restricted to a subset of macrophages, FHOD4, a formin from the same family, has a wider
324 distribution and higher expression levels in monocytes and DCs. As a consequence, we tested
325 the interaction between IRAP and FHOD4. Endogenous FHOD4, as well as a FHOD4-GFP
326 fusion protein interacted with IRAP as demonstrated by reciprocal co-immunoprecipitations
327 (**Fig. 8b** and **Supplementary Fig. 5a**) and by Duolink, an alternative method used to

investigate protein interaction *in situ* [24] (**Fig. 8c** and **Supplementary Fig. 5b**). Confocal microscopy showed that FHOD4 could be recruited to IRAP$^+$ vesicles, together with a vesicular actin coat labeled by phalloidin (**Fig. 8d**). These results suggested that FHOD4 could anchor IRAP$^+$ vesicles to the actin cytoskeleton.

To investigate if FHOD4-IRAP interaction was involved in TLR9 activation in DCs, we knocked-down FHOD4 expression using lentiviral transduction of shRNA in BM-DCs from TLR9-GFP transgenic mice. FHOD4 was reproducibly reduced by 95% (± 10%) in the cells transduced with two shRNA (17 and 20) targeting FHOD4 (**Fig. 8e**). In the absence of FHOD4 and CpG stimulation, 40% (± 5%) of the endogenous TLR9-GFP was found in the cleaved form (**Fig. 8f**). In agreement with the increased basal processing of TLR9-GFP, the GFP-fused TLR9 was found in lysosomes in FHOD4 depleted cells (**Fig. 8g**). Thus, TLR9 trafficking and processing were affected by FHOD4 depletion, like in the case of IRAP deletion.

Considering the impact of FHOD4 depletion on TLR9 localization, we expected to have an increased TLR9-driven inflammatory response in FHOD4 depleted BM-DCs. When incubated with CpG, FHOD4 depleted cells (wt-shFHOD4) secreted significantly more pro-inflammatory cytokines than the cells transduced with a non-targeting shRNA (wt-shNT) (**Fig. 8h** and **Supplementary Fig. 6a**). Depletion of FHOD1 did not affected TLR9-GFP localization or activation (**Supplementary Fig. 6c, d**), consistent with its very low levels of expression in BMDCs (**Supplementary Fig. 6b**). These results suggest that IRAP anchors endosomal vesicles to the actin cytoskeleton through its specific interaction with FHOD4, slowing their transport to lysosomes. A major effect of these molecular interactions is ensuring a limited interaction between TLR9 and its ligand, which prevents hyper-inflammation.

DISSCUSSION

The capacity of intracellular TLRs to recognize host nucleic acids is a risk for auto-immunity. For example, inappropriate activation of endosomal TLRs by self DNA has a major role in inflammation that occurs in systemic lupus erythematous, arthritis and psoriasis [34]. To avoid hyper-activation of TLRs, their encounter with the ligands and ability to signal must be tightly regulated. First, exposure to ligands is restricted through the retention of TLRs in the ER in basal conditions [35] and second, downstream signaling depends on the partial proteolysis of TLRs that occurs in the endo-lysosomal compartment [5,7,8,12,36]. Although these two steps apply to all intracellular TLRs, recent in-depth studies show that the trafficking routes used by

distinct endosomal TLRs to reach the endocytic pathway are different [5,6]. TLR9, like other TLRs, exits ER by interacting with Unc93b [35]. Unlike other TLRs, the TLR9-Unc93b complex reaches the cell surface and is later internalized into a poorly characterized endosomal compartment through AP-2 mediated endocytosis [6].

In this study, we identified IRAP as a regulator of CpG and TLR9 intracellular trafficking and *in vivo* activation of TLR9. IRAP deficiency led to rapid transport of internalized CpG to lysosomes and to TLR9 localization in lysosomes, where TLR9 is cleaved into its active C-ter form in the absence of CpG ligand. We observed this aberrant TLR9 trafficking and processing not only for TLR9-GFP, but also for endogenous TLR9 detected with anti-TLR9 antibodies. Lysosomal localization of TLR9 in IRAP-deficient cells might be a consequence of accelerated trafficking of its ligand, which normally is retained in $IRAP^+$ vesicles for a long time. The aberrant trafficking of both the ligand and the receptor led to an uncontrolled inflammatory response to TLR9 ligands, which culminated with animal death following an infection with *P. aeruginosa*, a bacterium sensed by TLR9 [26]. Altogether, our results show that IRAP is required to avoid excessive TLR9-driven inflammatory responses. In view of these results, it is conceivable that IRAP plays a role in human autoimmune pathologies through its effects on TLR9 signaling. The recent identification of a genetic association between psoriasis, one of the autoimmune disorders implicating TLR9 activation, and a nonsense mutation in the LNPEP gene encoding IRAP is consistent with this hypothesis [22].

The new role of IRAP and our co-localization experiments define an endosomal compartment that is described by the presence of Rab14 and Stx6 (**Supplementary Fig. 7**) and partially overlaps with $VAMP3^+$ and $EEA1^+$ vesicles. VAMP3 and TLR9 have been shown to co-localize in an intermediate step of the route that TLR9 follows towards lysosomes and which depends on the AP-3 adaptor [15]. Our data suggest that IRAP vesicles delay the trafficking of CpG and TLR9 from $EEA1^+$ endosomes to lysosomes, with important functional consequences. To understand how IRAP could mechanistically affect the dynamics of the early endosomal compartment in which CpG and TLR9 are retained, we screen for cytoskeletal proteins that might interact with IRAP and could interfere with endosomal motility. Indeed, considering that the cytosolic tail of IRAP was shown to interact with two cytoskeleton components, an actin nucleation factor, the formin FHOD1 [21] and the intermediate filament vimentin [20], we hypothesized that these interactions ensure the anchoring of IRAP and the associated TLR9 endosomes to cytoskeleton. Whereas the interaction of IRAP with vimentin was not detectable in DCs (experiments not shown), we found that IRAP binds to FHOD4 formin.

Formins are major actin nucleation factors that drive the assembly of actin monomers into filamentous structures and remain associated with the barbed end during filament elongation [37]. A knock-down of FHOD4 had effects similar to IRAP deletion on TLR9 trafficking and the cellular response to CpG. These results suggest that by promoting actin assembly on endosomes, FHOD4 prevents the transfer of endosomes to microtubules, delaying their retrograde transport towards lysosomes, as reported for the formin mDia1 [38]. Actin polymerization around the endosomal vesicles containing TLR9 ligands has been shown to be also driven by the other key actin nucleation factor, Arp2/3, and to be essential in limiting TLR9 signaling [39]. Interestingly, both, FHOD4 and Arp2/3 are activated by the same small GTPase of Rho family, Cdc42 [37], suggesting that these two actin-remodeling factors might cooperate in the regulation of TLR9 signaling, like they cooperate in phagocytic cup formation [40].

The intervention of FHOD4 in interaction with IRAP for modulating TLR9 function has major implications for potential links between extracellular stimuli, such as cytokines and the ability of TLR9 to respond to its ligands. It has been previously reported that TLR responses can be inhibited by extracellular stimuli such as cytokines [41] or integrin ligation [42,43]. Since Cdc42 activation occurs downstream integrin, receptor tyrosine kinase or G-protein-coupled receptors signaling [44], it could affect actin polymerization and the anchoring of $CpG^+/TLR9^+$ vesicles by IRAP. Thus, the anchoring of $CpG^+/TLR9^+$ vesicles to actin cytoskeleton could be essential in regulating TLR9 dependent cellular responses to the environment.

ACKNOWLEDGEMENTS

We are grateful to N. Goudin and S. Benadda for advice on analysis and quantification of confocal microscopy images, to S. Keller for anti-IRAP rabbit antibodies and mice, to D. Billadeau for anti-FHODs antibodies and to F. Benvenutti, F. Perez and S. Blystone for plasmid vectors. This work received financial support from the French “Agence Nationale de Recherche”, ANR IRAP-DC, ANR CytoEndoStor, ANR 2010 MIDI 008 01 and ANR post-doctoral support to D. D. We thank the Foundation “ARC pour la Recherche sur le cancer” for the acquisition of Leica SP8 confocal microscope and for the financial support to J.B.

Figure Legends

Figure 1. IRAP deletion increases TLR9 response

(**a**) Wt and IRAP-deficient (ko) BM-DCs were stimulated with different TLR ligands for 16 h and the secretion of IL-6, IL-12(p40) and TNF-α in supernatants was measured by ELISA (n=10 experiments, mean ± SEM, * p<0.05, ** p<0.01). (**b**) Wt and ko BM-DCs were incubated for 16 h with TLR ligands and IFN-β was measured by ELISA (n=3 experiments, **p<0.01). (**c-d**) Splenic cDCs (**c**) or pDCs (**d**) from wt and ko mice were isolated by cell sorting (**c**) or anti-PDCA-1 magnetic beads (**d**), incubated overnight with CpG-B or CpG-A and cytokine secretion was measured by ELISA (n=2 experiments, **p<0.001). (**e**) Wt and ko BM-DCs were incubated for 3 h with CpG-B or LPS and mRNA for TNF-α, IL-6 and IL-12 was quantified by RT-PCR using as reporters GAPDH and HPRT1. NS= non-stimulated cells. (n= 4 experiments, data are represented as means ± SEM, * p<0.05, ** p<0.01). (**f**) mRNAs for IL-6 and IL-12 from wt and ko splenic pDCs, stimulated or not (NS) with CpG-B, were measured by RT-PCR using the same reporter genes as in **e** (n= 3 experiments, means ± SEM, * p<0.05). See also **Supplementary Fig. 1**.

Figure 2. Increased TLR9 signaling in IRAP-deficient DCs

PLA for detection of MyD88/NF-κB (**a**) or MyD88/IRF7 (**b**) proximity was performed with specific antibodies against MyD88, NF-κB and IRF7. The graphs show the quantification of MyD88 interaction with NF-κB (**a**) or IRF7 (**b**) by PLA. A minimum of 30 cells was analyzed in each condition. (n=3 experiments, means ± SD, ** p<0.01, ***p<0.001). Statistical analysis was performed with Student t test. (**c-d**) Wt or ko BMDCs were incubated with TLR ligands (CpG-B: 10 µg/ml, LPS: 100 ng/ml) for 10, 20, 30, 40, 60 and 120 minutes. Cells lysates were assessed for ERK (**c**) and I-KB-α (**d**) phosphorylation by Western Blot and ELISA. Total ERK (t-ERK) and I-KB-α (t-I-KB-α) were also measured. Phosphorylated ERK (p-ERK) proteins were quantified and normalized over total ERK (t-ERK) using IMAGE J software. (**c**, **d**, n= 3 experiments, means ± SEM, * p<0.05, ** p<0.01, *** p<0.001, **** p<0.0001).

Figure 3. IRAP-deficient mice display a hyper-inflammatory phenotype driven by TLR9 activation

(**a**) IL-6 production was measured in serum of wt or IRAP-deficient (ko) mice 2 h after i.v. injection of CpG-B (left panel) or LPS (right panel) (n=9 animals, mean ± SEM, ** p<0.01).

(**b**) Wt and ko mice (n=9-11 in each group), were inoculated intranasally with *P. Aeruginosa* at 10^6 cfu/mouse. Animal survival was determined up to 7 days post-infection (n=3 independent experiments, * p<0.05). (**c**) Broncho-alveolar lavage (BAL) fluid levels of KC, IL-6, TNF-α and IL-1β in wt and ko mice 24 h after intranasal inoculation of *P. Aeruginosa* (10^6 cfu/mice) (n=9 animals, 3 independent experiments, mean ± SEM * p<0.05, ** p<0.01, *** p<0.001). (**d**) TNF-α, KC and IL-6 secretion in supernatants of non-stimulated (NS), CpG-B- or LPS-stimulated wt or ko alveolar macrophages (2 independent experiments, mean ± SEM, * p<0.05, *** p<0.001. (**e**) Twenty-four hours post-infection, bacterial load was determined in lungs from wt and ko mice. (n=9 animals; graphs show mean ± SEM of 2 independent experiments). See also **Supplementary Fig. 2**.

Figure 4. IRAP enzymatic activity is not involved in TLR9 activation

(**a**) IRAP-deficient (ko) BM-DCs reconstituted with active or inactive IRAP-HA by nucleofection were seeded on fibronectin-coated slides and stained with anti-Stx6 and anti-HA specific antibodies. The graph shows the colocalization between IRAP and Stx6 (n=10 cells, two experiments). (**b**) IRAP-deficient fibroblasts were transfected by electroporation with active or inactive IRAP and 36 h later, IRAP expression was analyzed by immunoblotting with anti-IRAP antibodies. (**c**) IRAP was immunoprecipitated with anti-IRAP antibodies from the fibroblasts transfected as in (**b**) and the aminopeptidase activity was tested by incubation of the beads with the colorimetric substrate Leu-AMC (2 independent experiments). (**d-e**) IRAP-deficient BM-DCs reconstituted with active (**d**) or inactive (**e**) IRAP were stimulated with TLR ligands for 16 h and IL-6 secretion was measured by ELISA (three (**d**) or two (**e**) independent experiments, mean ± SEM, **p<0.01, ***p<0.001).

Figure 5. CpG and TLR9 are cargos of IRAP endosomes

(**a**) Wt BM-DCs were pulsed for 20 minutes with CpG-FITC, chased at 37°C for the indicated time-points, washed in PBS, fixed and stained with anti-IRAP and anti-FITC specific antibodies. (**b**) Wt BM-DCs were transfected with TLR9-GFP by nucleofection. Two days later, the cells were stimulated or not with CpG-B for 20 min, fixed and stained with anti-IRAP specific antibodies. See also **Supplementary Fig. 3**.

Figure 6. IRAP absence increases the susceptibility of TLR9 to lysosomal processing

(**a**) Wt and IRAP-deficient BM-DCs were pulsed for 20 minutes with CpG-FITC, chased at

37°C for the indicated time-points, washed in PBS, fixed and stained with anti-LAMP1 and anti-FITC specific antibodies (2 experiments, n=6 cells, *p<0.05, ***p<0.001). (**b**) IRAP-deficient and wt BM-DCs were transfected with TLR9-GFP by nucleofection and 48 h later stimulated or not with CpG-B for 20 or 120 min. The cells were fixed and stained with specific antibodies for LAMP1 (2 experiments, n=10 cells, *p<0.05, **p<0.01). (**c**) Wt and IRAP-deficient fibroblasts expressing TLR9-GFP and Unc93b-Cherry were lysed in 1% NP-40 and TLR9-GFP was immunoprecipitated with anti-GFP antibodies and analyzed by anti-GFP immunoblot. One experiment out of three is shown. The graph represents the quantification of GFP immunoblots from the three independent experiments. Phagosomes from wt, ko (**e**) and $tlr9^{-/-}$ (TLR9-ko, **d**) BMDCs unstimulated or stimulated with CpG-B (10 µg/ml) were magnetically purified after 20 min or 120 min. Proteins expressed in phagosomes (10 µg) were resolved by SDS-PAGE and endogenous TLR9 and LAMP1 proteins were visualized by immunoblot. Data are representative of two experiments.

Figure 7. IRAP deletion reduces CpG and TLR9 retention in early endosomes

BM-DCs from TLR9-GFP transgenic mice were transduced with a lentivirus coding for a shRNA against IRAP (shIRAP) or a non-targeting shRNA (shNT). (**a**) The cells were pulsed or not with Biotinylated-CpG, washed and chased for the indicated time points. After fixation, the cells were stained with anti-EEA1 specific antibodies. (**b**) The graphs represent the percentage of colocalization between the proteins visualized in (**a**) (2 experiments, n=6 cells, *p<0.05, **p<0.01, ***p<0.001 ****p<0.0001). (**c**) CpG-FITC up-take by wt and IRAP-deficient BM-DCs was measured by flow cytometry. (**d**) The efficiency of IRAP knockdown was analyzed by immunoblotting, using anti-IRAP antibodies and anti α-Tubulin antibodies for the loading control.

Figure 8. IRAP interaction with the FHOD family of formins controls TLR9 activation

(**a**) *IRAP (encoded by Lnpep gene)*, *FHOD1*, *FHOD4* and *TLR9* mRNA expression data were recovered from immgen (https://www.immgen.org/Databrowserpage.swf) for pDCs (pDCs_8+_sp sub-type), Monocytes (Mo_C6+_II+_Bl type) and Macrophages (MF_RP_Sp type). (**b**) Endogenous IRAP and FHOD4 were immunoprecipitated with antibodies anti-IRAP and anti-FHOD4 respectively and the precipitates were split in two and analyzed by immunoblot as indicated. (**c**) In situ IRAP/FHOD4 interaction was detected by Duolink assay in wt and IRAP-deficient (ko) BM-DCs using antibodies against IRAP and FHOD4 (2

independent experiments, 10 cells acquired). (**d**) Wt fibroblasts expressing FHOD4-GFP were fixed and stained with phalloidin and anti-IRAP antibodies. 40% (+/-5) of IRAP colocalized with FHOD4 (n=5 cells, 2 independent experiments). (**e-g**) BM-DCs from TLR9-GFP transgenic mice were transduced with two lentiviruses coding for shRNAs against *FHOD4* (shFHOD4 17 and shFHOD4 20) or a non-targeting shRNA (shNT). (**e**) The efficiency of FHOD4 knock-down was analyzed by immunoblotting using anti FHOD4 antibodies. (**f**) Endogenous TLR9-GFP processing in cells transduced with shNT or shFHOD4 (20) was analyzed by immunoblot with anti-GFP antibodies. Control corresponds to untransduced wt BMDCs. (**g**) Endogenous TLR9-GFP localization in steady state conditions was analyzed by confocal microscopy using an anti-LAMP1 antibody. The graph represents the quantification of TLR9-GFP/LAMP1 colocalization (2 experiments, n=10 cells, ***p<0.001). (**h**) Wt and ko BMDCs were transduced with shNT (non-targeting) and shFHOD4 (20) lentiviruses and stimulated with different TLR ligands for 6 h. The secretion of IL-12(p40) in supernatants was measured by ELISA (n=3 experiments, mean ± SEM, **p<0.01, *p<0.05). See also **Supplementary Fig. 5-6.**

References

1 Lee, B. L. & Barton, G. M. Trafficking of endosomal Toll-like receptors. *Trends in cell biology* 24, 360-369, doi:10.1016/j.tcb.2013.12.002 (2014).

2 Latz, E. *et al*. TLR9 signals after translocating from the ER to CpG DNA in the lysosome. *Nat Immunol* 5, 190-198, doi:10.1038/ni1028 (2004).

3 Leifer, C. A. *et al*. TLR9 is localized in the endoplasmic reticulum prior to stimulation. *J Immunol* 173, 1179-1183 (2004).

4 Fukui, R. *et al*. Unc93B1 restricts systemic lethal inflammation by orchestrating Toll-like receptor 7 and 9 trafficking. *Immunity* 35, 69-81, doi:10.1016/j.immuni.2011.05.010 (2011).

5 Garcia-Cattaneo, A. *et al*. Cleavage of Toll-like receptor 3 by cathepsins B and H is essential for signaling. *Proc Natl Acad Sci U S A* 109, 9053-9058, doi:10.1073/pnas.1115091109 (2012).

6 Lee, B. L. *et al*. UNC93B1 mediates differential trafficking of endosomal TLRs. *Elife* 2, e00291, doi:10.7554/eLife.00291 (2013).

7 Asagiri, M. *et al*. Cathepsin K-dependent toll-like receptor 9 signaling revealed in experimental arthritis. *Science* 319, 624-627, doi:10.1126/science.1150110 (2008).

8 Ewald, S. E. *et al*. Nucleic acid recognition by Toll-like receptors is coupled to stepwise processing by cathepsins and asparagine endopeptidase. *J Exp Med* 208, 643-651, doi:10.1084/jem.20100682 (2011).

9 Hipp, M. M. *et al*. Processing of human toll-like receptor 7 by furin-like proprotein convertases is required for its accumulation and activity in endosomes. *Immunity* 39, 711-721, doi:10.1016/j.immuni.2013.09.004 (2013).

10 Maschalidi, S. *et al*. Asparagine endopeptidase controls anti-influenza virus immune responses through TLR7 activation. *PLoS Pathog* 8, e1002841, doi:10.1371/journal.ppat.1002841 (2012).

11 Park, B. *et al*. Proteolytic cleavage in an endolysosomal compartment is required for activation of Toll-like receptor 9. *Nat Immunol* 9, 1407-1414, doi:10.1038/ni.1669 (2008).

12 Sepulveda, F. E. *et al*. Critical role for asparagine endopeptidase in endocytic Toll-like receptor signaling in dendritic cells. *Immunity* 31, 737-748, doi:10.1016/j.immuni.2009.09.013 (2009).

13 Hayashi, K., Sasai, M. & Iwasaki, A. Toll-like receptor 9 trafficking and signaling for type I interferons requires PIKfyve activity. *Int Immunol* 27, 435-445, doi:10.1093/intimm/dxv021 (2015).

14 Hazeki, K., Uehara, M., Nigorikawa, K. & Hazeki, O. PIKfyve regulates the endosomal localization of CpG oligodeoxynucleotides to elicit TLR9-dependent cellular responses. *PLoS One* 8, e73894, doi:10.1371/journal.pone.0073894 (2013).

15 Sasai, M., Linehan, M. M. & Iwasaki, A. Bifurcation of Toll-like receptor 9 signaling by adaptor protein 3. *Science* 329, 1530-1534, doi:10.1126/science.1187029 (2010).

16 Saveanu, L. *et al*. IRAP identifies an endosomal compartment required for MHC class I cross-presentation. *Science* 325, 213-217, doi:10.1126/science.1172845 (2009).

17 Weimershaus, M. *et al*. Conventional dendritic cells require IRAP-Rab14 endosomes for efficient cross-presentation. *J Immunol* 188, 1840-1846, doi:10.4049/jimmunol.1101504 (2012).

18 Keller, S. R., Scott, H. M., Mastick, C. C., Aebersold, R. & Lienhard, G. E. Cloning and characterization of a novel insulin-regulated membrane aminopeptidase from Glut4 vesicles. *J Biol Chem* 270, 23612-23618 (1995).

19 Hosaka, T. *et al*. p115 Interacts with the GLUT4 vesicle protein, IRAP, and plays a critical role in insulin-stimulated GLUT4 translocation. *Mol Biol Cell* 16, 2882-2890, doi:10.1091/mbc.E05-01-0072 (2005).

20 Hirata, Y. *et al*. Vimentin binds IRAP and is involved in GLUT4 vesicle trafficking. *Biochem Biophys Res Commun* 405, 96-101, doi:10.1016/j.bbrc.2010.12.134 (2011).

21 Tojo, H. *et al*. The Formin family protein, formin homolog overexpressed in spleen, interacts with the insulin-responsive aminopeptidase and profilin IIa. *Mol Endocrinol* 17, 1216-1229, doi:10.1210/me.2003-0056 (2003).

22 Cheng, H. *et al*. Identification of a missense variant in LNPEP that confers psoriasis risk. *J Invest Dermatol* 134, 359-365, doi:10.1038/jid.2013.317 (2014).

23 Stow, J. L., Low, P. C., Offenhauser, C. & Sangermani, D. Cytokine secretion in macrophages and other cells: pathways and mediators. *Immunobiology* 214, 601-612, doi:10.1016/j.imbio.2008.11.005 (2009).

24 Leuchowius, K. J., Weibrecht, I. & Soderberg, O. In situ proximity ligation assay for microscopy and flow cytometry. *Curr Protoc Cytom* Chapter 9, Unit 9 36, doi:10.1002/0471142956.cy0936s56 (2011).

25 Greene, C. M. *et al*. TLR-induced inflammation in cystic fibrosis and non-cystic fibrosis airway epithelial cells. *J Immunol* 174, 1638-1646 (2005).

26 Benmohamed, F. *et al*. Toll-Like Receptor 9 Deficiency Protects Mice against Pseudomonas aeruginosa Lung Infection. *PLoS One* 9, e90466, doi:10.1371/journal.pone.0090466 (2014).

27 Saveanu, L. & van Endert, P. The role of insulin-regulated aminopeptidase in MHC class I antigen presentation. *Front Immunol* 3, 57, doi:10.3389/fimmu.2012.00057 (2012).

28 Onji, M. *et al*. An essential role for the N-terminal fragment of Toll-like receptor 9 in DNA sensing. *Nat Commun* 4, 1949, doi:10.1038/ncomms2949 (2013).

29 Fratti, R. A., Backer, J. M., Gruenberg, J., Corvera, S. & Deretic, V. Role of phosphatidylinositol 3-kinase and Rab5 effectors in phagosomal biogenesis and mycobacterial phagosome maturation arrest. *J Cell Biol* 154, 631-644, doi:10.1083/jcb.200106049 (2001).

30 Lakadamyali, M., Rust, M. J. & Zhuang, X. Ligands for clathrin-mediated endocytosis are differentially sorted into distinct populations of early endosomes. *Cell* 124, 997-1009, doi:10.1016/j.cell.2005.12.038 (2006).

31 Kim, S. & Coulombe, P. A. Intermediate filament scaffolds fulfill mechanical, organizational, and signaling functions in the cytoplasm. *Genes Dev* 21, 1581-1597, doi:10.1101/gad.1552107 (2007).

32 Goode, B. L. & Eck, M. J. Mechanism and function of formins in the control of actin assembly. *Annu Rev Biochem* 76, 593-627, doi:10.1146/annurev.biochem.75.103004.142647 (2007).

33 Heng, T. S. & Painter, M. W. The Immunological Genome Project: networks of gene expression in immune cells. *Nat Immunol* 9, 1091-1094, doi:10.1038/ni1008-1091 (2008).

34 Rifkin, I. R., Leadbetter, E. A., Busconi, L., Viglianti, G. & Marshak-Rothstein, A. Toll-like receptors, endogenous ligands, and systemic autoimmune disease. *Immunological reviews* 204, 27-42, doi:10.1111/j.0105-2896.2005.00239.x (2005).

35 Brinkmann, M. M. *et al*. The interaction between the ER membrane protein UNC93B and TLR3, 7, and 9 is crucial for TLR signaling. *J Cell Biol* 177, 265-275, doi:10.1083/jcb.200612056 (2007).

36 Descamps, D. *et al*. Toll-like receptor 5 (TLR5), IL-1beta secretion, and asparagine endopeptidase are critical factors for alveolar macrophage phagocytosis and bacterial killing. *Proc Natl Acad Sci U S A* 109, 1619-1624, doi:10.1073/pnas.1108464109 (2012).

37 Kuhn, S. & Geyer, M. Formins as effector proteins of Rho GTPases. *Small GTPases* 5, e29513, doi:10.4161/sgtp.29513 (2014).

38 Fernandez-Borja, M., Janssen, L., Verwoerd, D., Hordijk, P. & Neefjes, J. RhoB regulates endosome transport by promoting actin assembly on endosomal membranes through Dia1. *Journal of cell science* 118, 2661-2670, doi:10.1242/jcs.02384 (2005).

39 Prete, F. *et al*. Wiskott-Aldrich syndrome protein-mediated actin dynamics control type-I interferon production in plasmacytoid dendritic cells. *J Exp Med* 210, 355-374, doi:10.1084/jem.20120363 (2013).

40 Seth, A., Otomo, C. & Rosen, M. K. Autoinhibition regulates cellular localization and actin assembly activity of the diaphanous-related formins FRLalpha and mDia1. *J Cell Biol* 174, 701-713, doi:10.1083/jcb.200605006 (2006).

41 Wimmer, N. *et al*. Lymphotoxin beta receptor activation on macrophages induces cross-tolerance to TLR4 and TLR9 ligands. *J Immunol* 188, 3426-3433, doi:10.4049/jimmunol.1103324 (2012).

42 Acharya, M. *et al*. alphav Integrins combine with LC3 and atg5 to regulate Toll-like receptor signalling in B cells. *Nat Commun* 7, 10917, doi:10.1038/ncomms10917 (2016).

43 Han, C. *et al*. Integrin CD11b negatively regulates TLR-triggered inflammatory responses by activating Syk and promoting degradation of MyD88 and TRIF via Cbl-b. *Nat Immunol* 11, 734-742, doi:10.1038/ni.1908 (2010).

44 Etienne-Manneville, S. Cdc42--the centre of polarity. *Journal of cell science* 117, 1291-1300, doi:10.1242/jcs.01115 (2004).

666
667

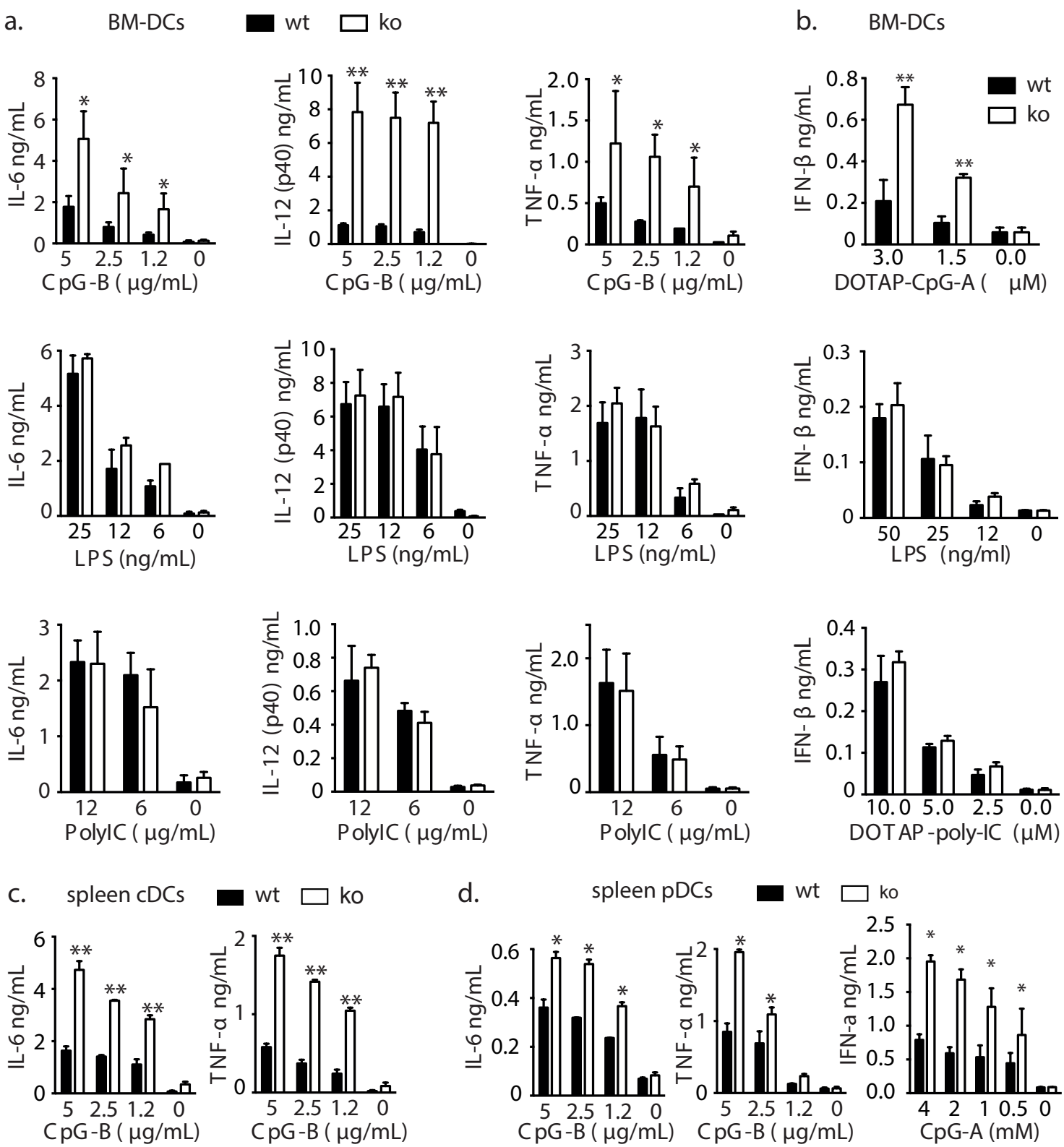

Figure 1 Babdor et al.

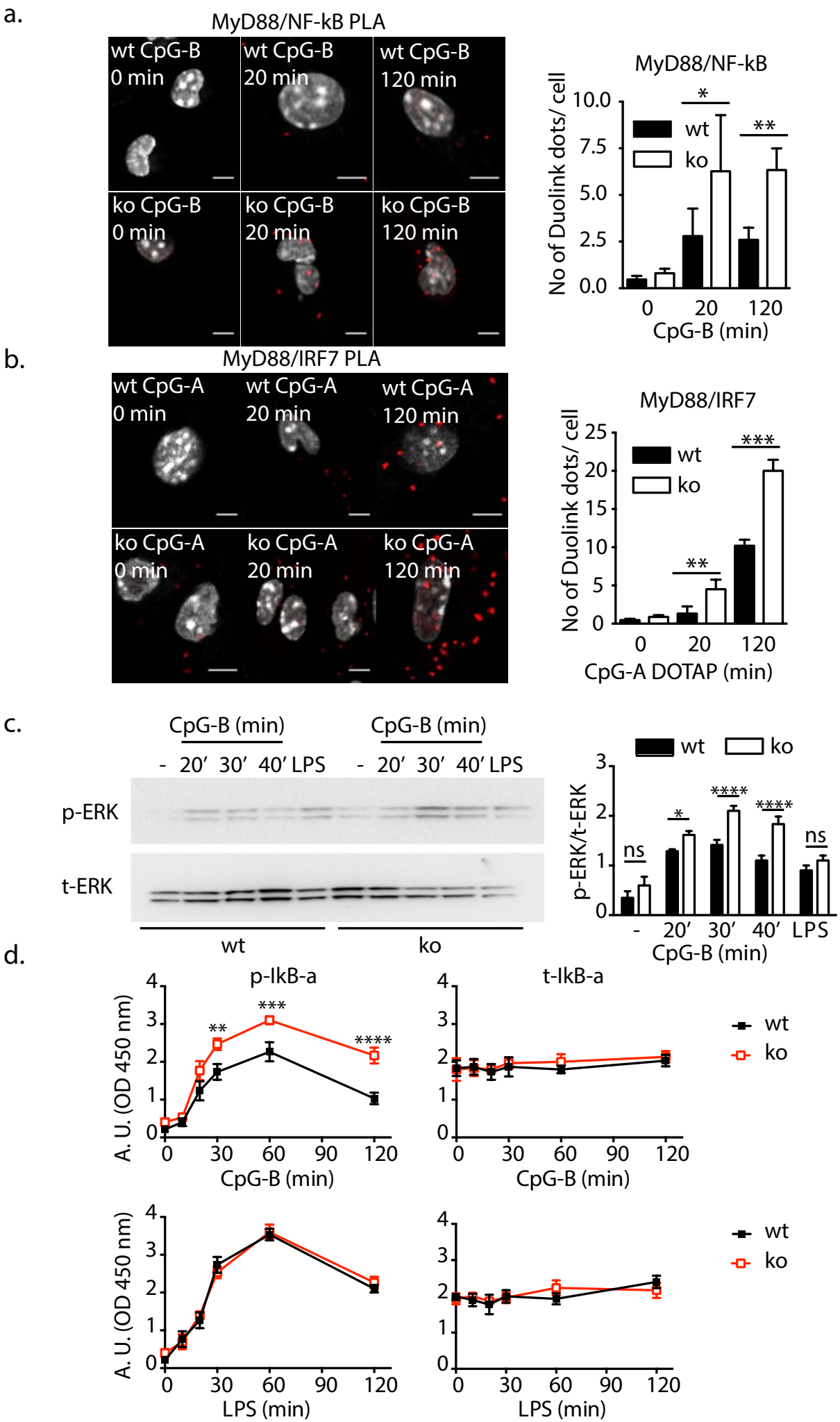

Figure 2. Babdor et al.

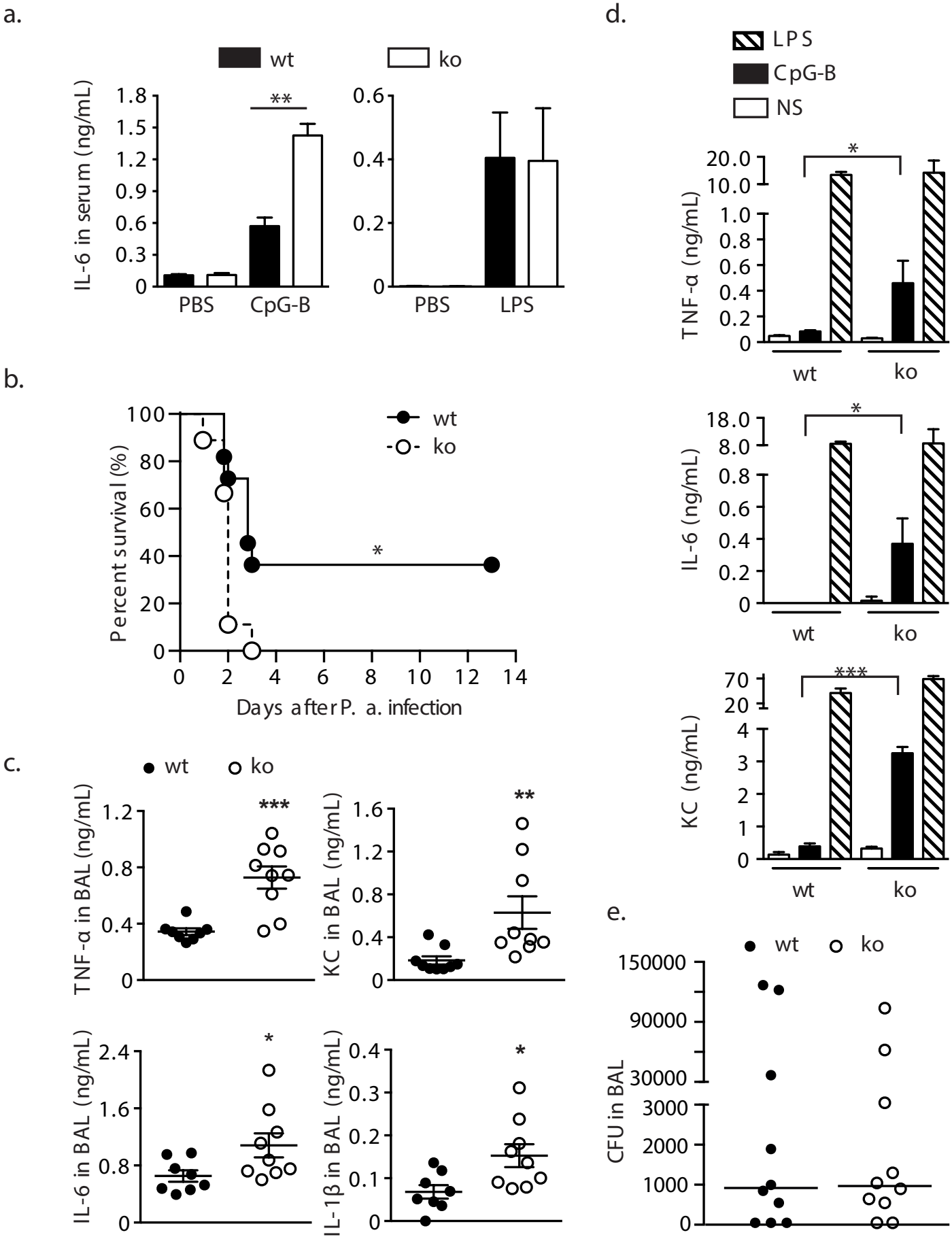

Figure 3. Babdor et al.

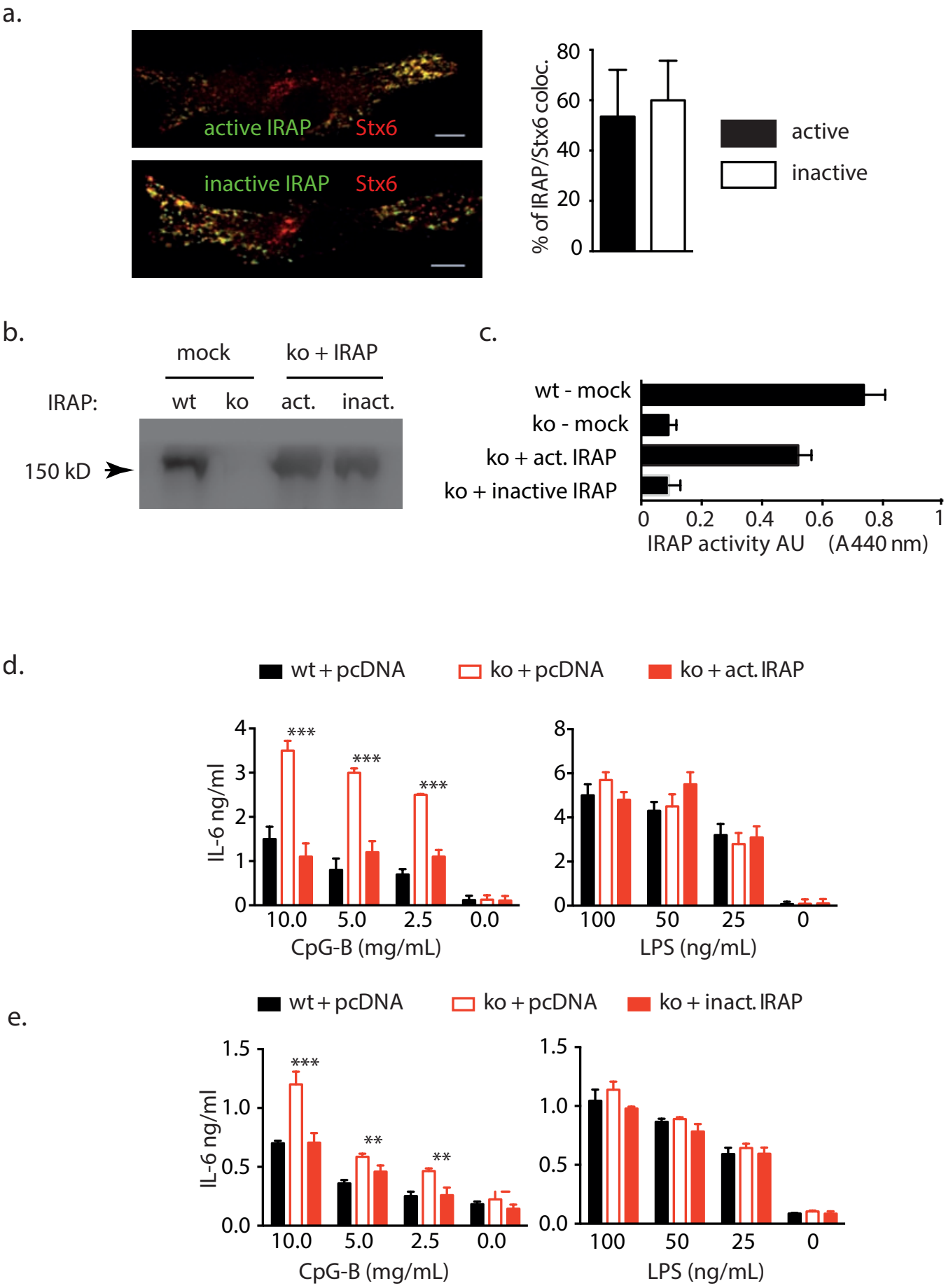

Figure 4. Babdor et al

a.

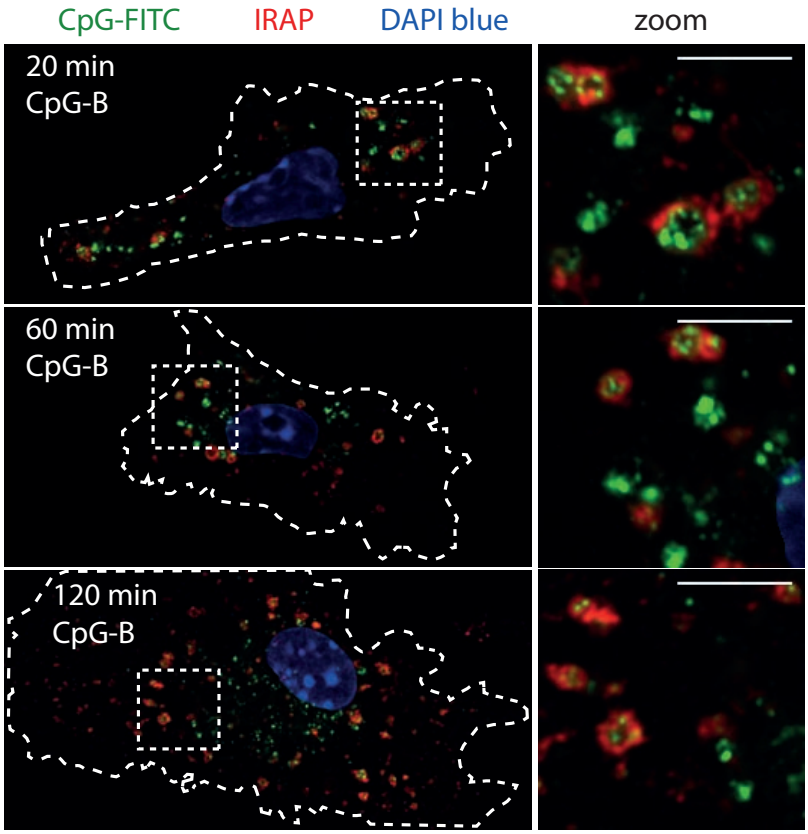

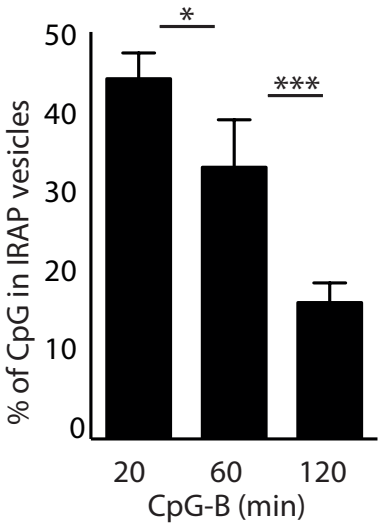

b.

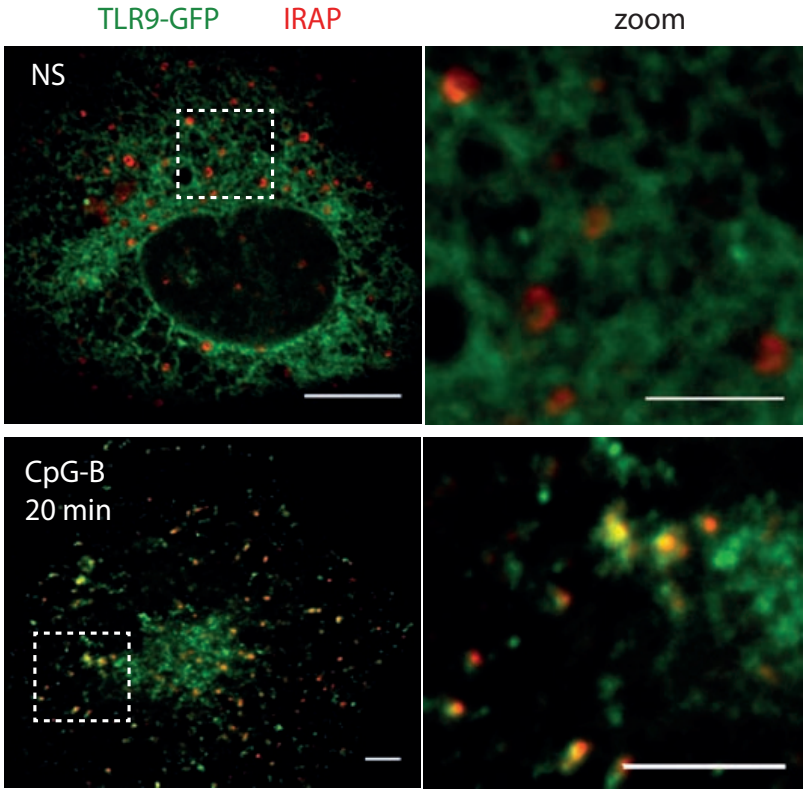

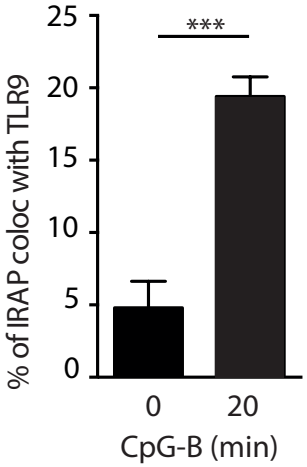

Figure 5 Babdor et al.

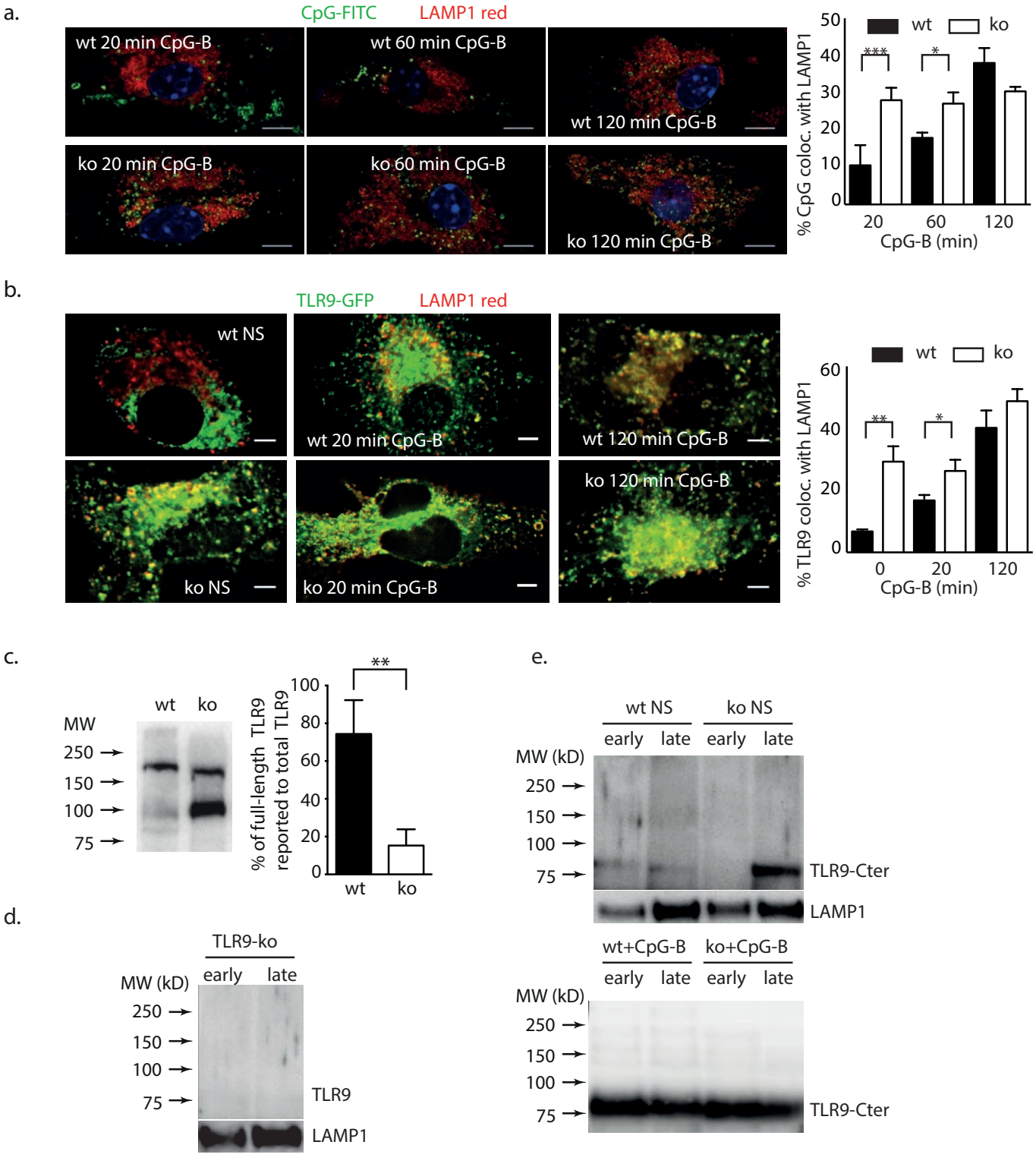

Figure 6_ Babdor et al.

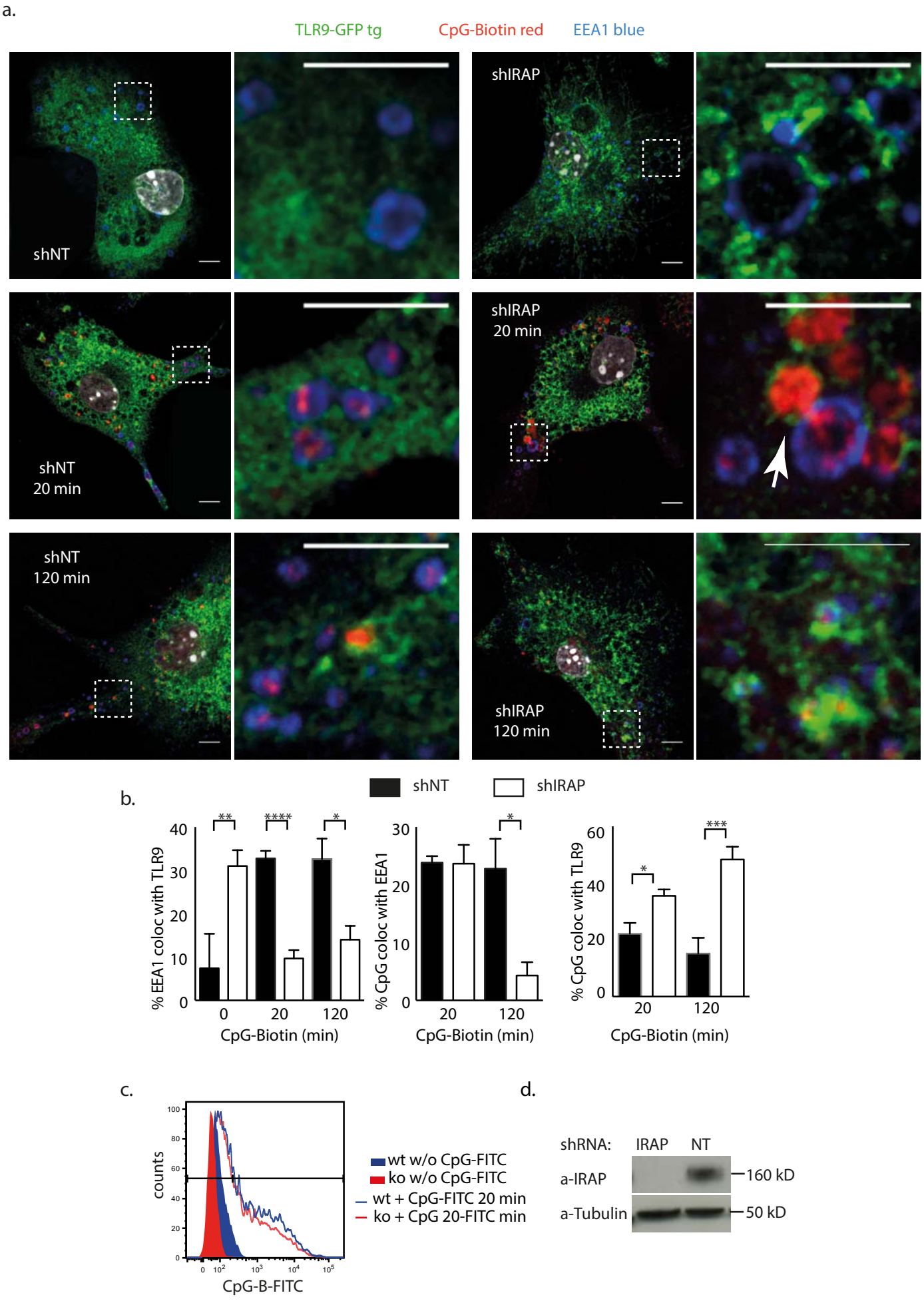

Figure 7 Babdor et al.

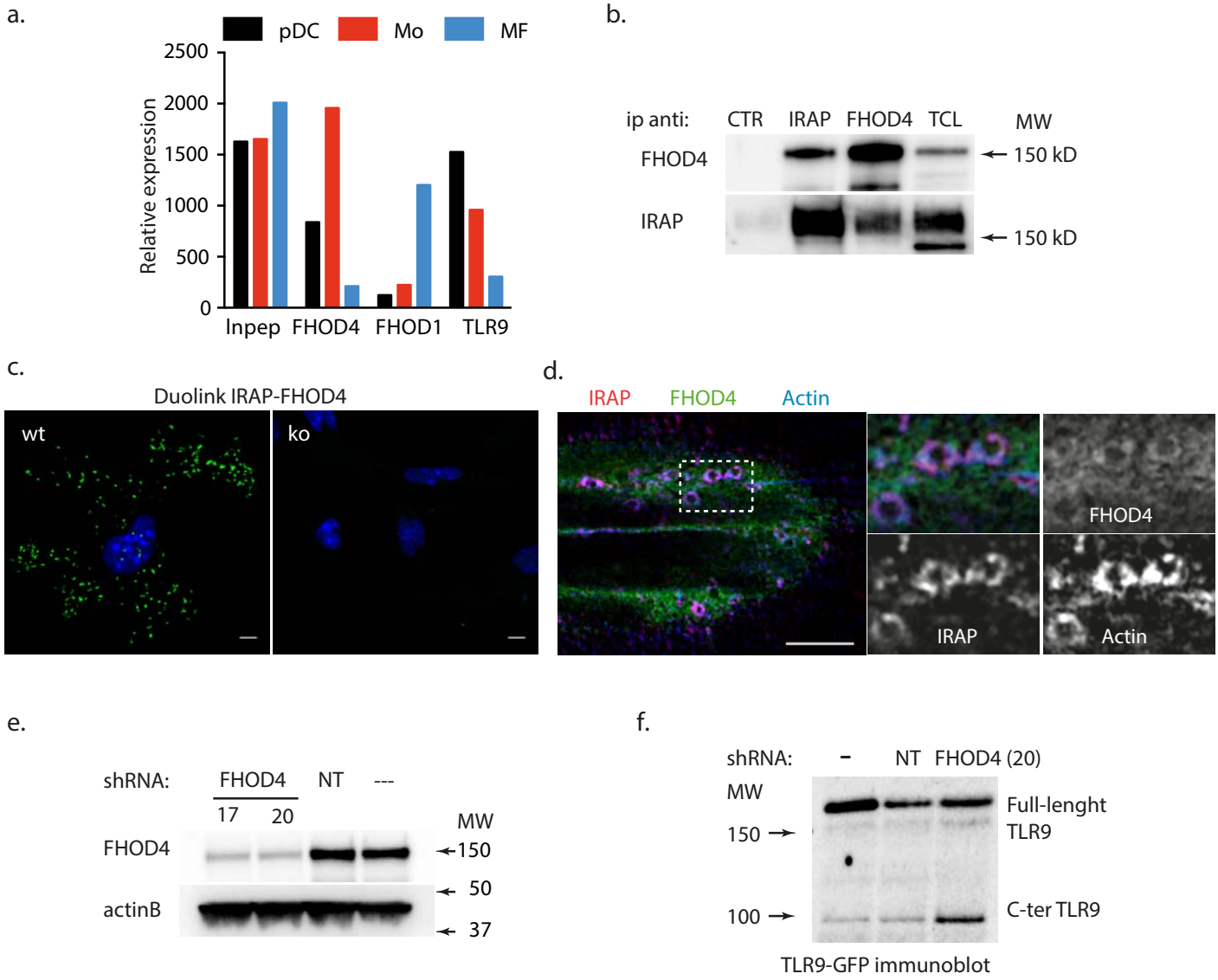

Figure 8 Babdor et al.